The International Journal of Advanced Manufacturing Technology (2018) 96:3585–3601
https://doi.org/10.1007/s00170-018-1788-1

ORIGINAL ARTICLE

# Free-bending process characteristics and forming process design of copper tubular components

Xunzhong Guo[1] · Hao Xiong[1] · Yong Xu[2] · Yannan Ma[1] · Ali Abd El-Aty[2] · Jie Tao[1] · Kai Jin[3]

Received: 6 November 2017 / Accepted: 12 February 2018 / Published online: 9 March 2018


## Abstract

Three-dimensional free-bending is a new and an advanced forming technology to manufacture the complex metal hollow components with continuously varying radius. In this study, the principle, process analysis, and the CNC control of free-bending were introduced in detail. The characteristics of the free-bending process, such as the motion trace scope of bending die and the stress variation in the free-bending process, were numerically investigated through finite element method using ABAQUS finite element code. With the simulation model, the material correction factor (Km) of copper was determined and the correction factor (Kc) for the clearance between the tube and bending die was also proposed. Moreover, the effects of the key process parameters including the clearance between the tube and bending die ($\Delta c$), the distance between the center of the bending die and the head of guide sleeve (A), and the axial feeding velocity (v) on the forming quality of the tubular bending components were studied as well. Through the finite element simulation and analysis, the optimum parameters (Km, Kc, $\Delta c$, A, and v) used in the free-bending process of the tubular component are summarized and the forming process design of the copper tubular component was also obtained. Based on the forming process design, the simulation and bending test of the copper tubular component were carried out, and the dimensions of the bending components gave a very good agreement with the results obtained from finite element modeling. Furthermore, there was no obvious cross section distortion, excessive thickening, and thinning of wall thickness of the formed tubular components. It is concluded that the three-dimensional free-bending technology is a novel forming process used to manufacture a sound complex three-dimensional hollow component with asymmetric cross sections and continuous varying radii.

**Keywords** Free-bending · Finite element analysis · Forming process design · Correction factor · Optimization of process parameters · Motion trajectory of the bending die

## 1 Introduction

Recently, the spot welded and stamped structural components in chassis and space frames have been increasingly replaced by hollow profiles [1]. The use of hollow structural sections allows for both weight and space saving but without sacrificing component strength and stiffness [2]. The demand of bent hollow components in different industrial sectors increases because of lightweight design, space, and cost saving [3]. The three-dimensional (3D) complex metal hollow components are widely used in the fuel, lubricating oil, hydraulic, and ring control systems which are mainly responsible for the transportation of critical media [4, 5]. Generally, the components in those systems are

✉ Yong Xu
yxu@imr.ac.cn

✉ Kai Jin
jinkai@nuaa.edu.cn

[1] Present address: College of Material Science and Technology, Nanjing University of Aeronautics and Astronautics, Nanjing 211100, People's Republic of China

[2] Institute of Metal Research, Chinese Academy of Sciences, Shenyang 110016, People's Republic of China

[3] College of Mechanical and Electrical Engineering, Nanjing University of Aeronautics and Astronautics, Nanjing 210016, People's Republic of China

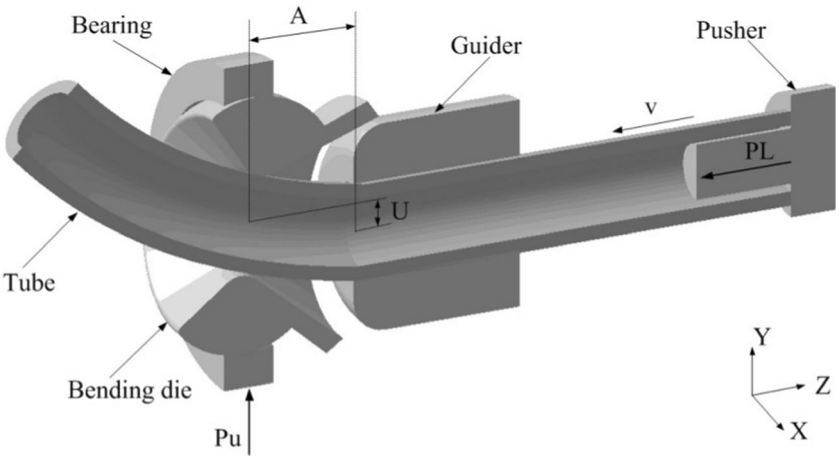


**Fig. 1** Schematic diagram of 3D free-bending principle

complex in shape, showing a variety of spatial configuration and continuous varying radius [6, 7]. The conventional bending processes such as push bending, stretch bending, and rotary draw bending are often unsuitable for complex geometries because the final forming geometry is defined by the geometry of the bending die [8]. Accordingly, the bending die must be changed frequently to fabricate those complex geometries. In addition, the component manufactured by mentioned bending processes tend to be pre-damaged due to clamping which can lead to failures during the downstream hydroforming process [9].

The 3D free-bending technology is a novel forming technology used to manufacture a sound complex 3D hollow component with asymmetric cross sections and continuous varying radius because of its geometrical flexibility and efficiency [10]. For the 3D free-bending technology, the bending die is actively shifted by two servo motors in the X and Y directions, and the tipping around its center is done by a spherical connection of the bending die to the guider. The pusher which feeds the tube in the Z direction is thereby synchronized with the X and Y axes of the bending die, and the forming geometry of free-bending process is defined by the offset of the bending die. Therefore, tubes with different radius can be manufactured without changing the die and re-clamping. Simultaneously, the uniformity of wall thickness and the flatness of cross section are improved due to the axial push force in the free-bending process.

In this study, the 3D bending process was investigated through the finite element method (FEM) using the ABAQUS finite element code. The motion trace scope of the bending die and stress variation in the free-bending process were identified. The material correction factor (Km) of copper and the correction factor (Kc) for the clearance between the tube and bending die were determined. Afterwards, the influences of the key process parameters including the clearance between the tube and the bending die (Δc), the distance between the center of the bending die and the head of guide sleeve (A), and the axial feeding velocity (v) on the forming quality of the 3D tubular bending components were investigated as well. Based on the above work, the forming process design of the copper tubular component was completed including the optimal process parameters and the determination of the motion trajectory of the bending die. Finally, the simulation and bending test of the copper tubular component were carried out based on the forming process design, and the bending tests and the simulation results are compared and analyzed.

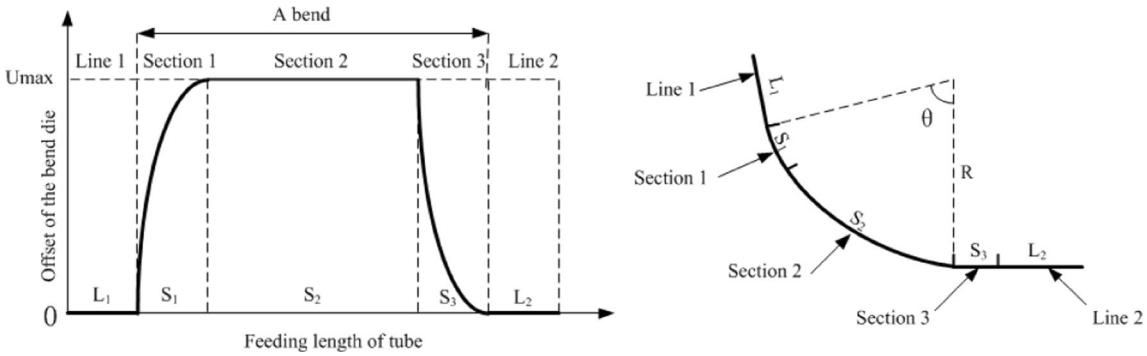


**Fig. 2** Three sections of the bending tube in free-bending forming process

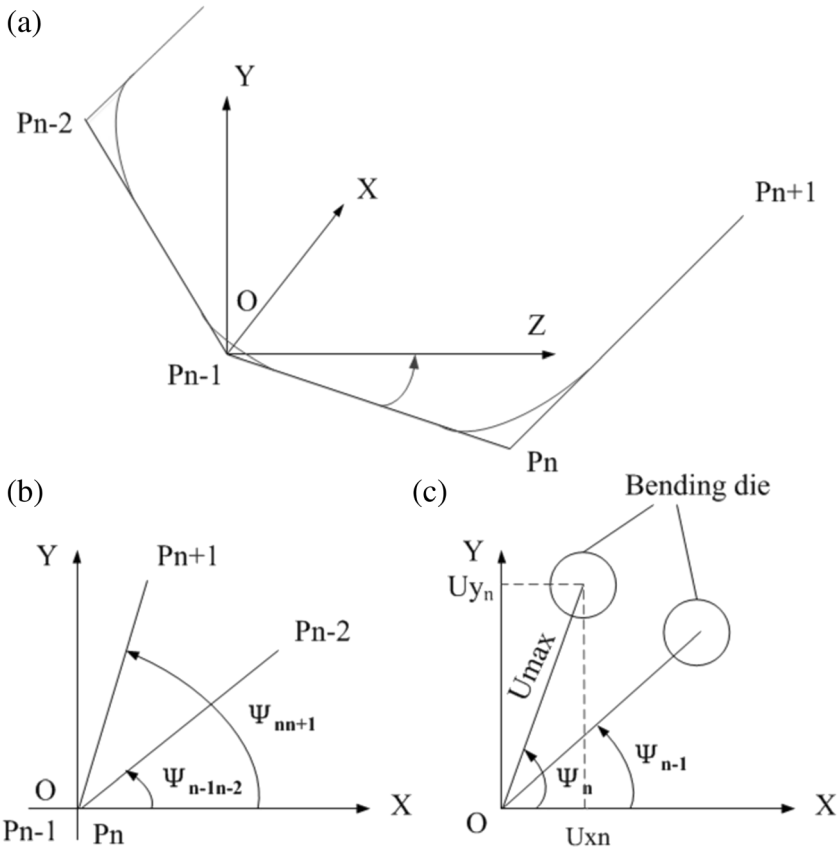


**Fig. 3** Example of bending direction

## 2 Free-bending technology

The three Japanese researchers namely Makoto Murata, Shinji Ohashi, and Hideo Suzuki proposed the principle of the 3D free-bending method called MOS bending. The principle of free-bending is adjusting the position of the bending die penetrated by tubes or profiles to bend tubes or profiles with different radius without changing the die and re-clamping [11–13]. Gantner [14] investigated the free-bending process by carrying out the finite element simulation and experiments which was also based on the same bending principle. The results obtained from experiments showed a little difference from that gained from simulation. Three-axis bending and five-axis bending kinematic and mathematical models were also presented by Gantner. In his investigation, the equation on the relationship between the offset (U) of the bending die and the bending radius (R) and the calculation formulas of the transition sections were put forward [15]. In recent years, a number of enterprises in Japan and Germany developed the different types of commercial free-bending forming equipment. By using these advanced free-bending machines, the minimum bending radius could reach to two times the outer tube diameter and the maximum feed rate of pipe exceeded 350 mm/s [16].


**Fig. 4** 3D free-bending CNC Tube Bender

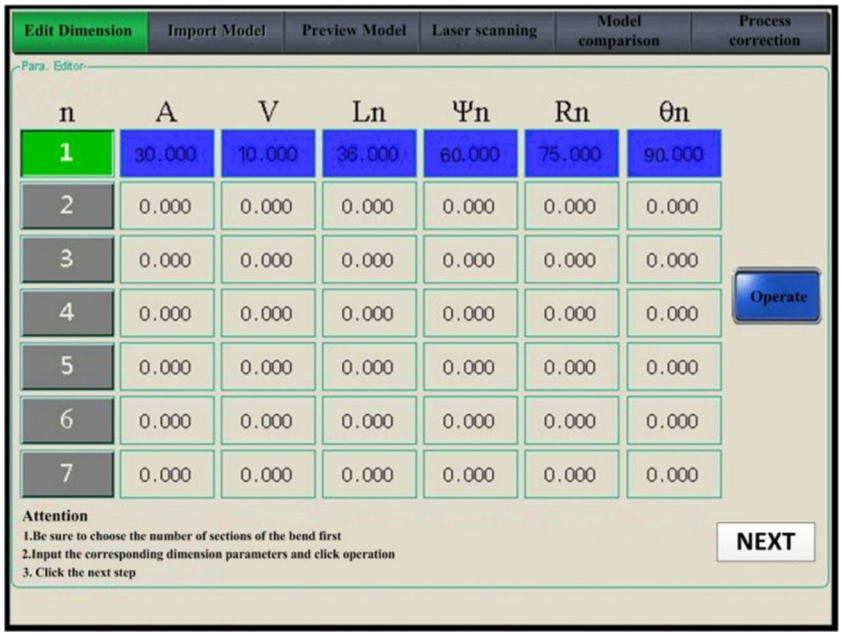


**Fig. 5** Entering data for the three-axis free-bending

## 2.1 Principle of free-bending

The technical principle of the 3D free-bending is shown in Fig. 1. The relative distance between the central axis of the guider and the central axis of the bending die in the Y direction is called offset (U) which often changes during the forming process. The distance between the center of the bending die and the exit of the guider is called approach (*A*) which is a set value in the forming process.

In the free-bending process, a tubular blank is penetrated into the bending die with a certain feeding velocity (*v*) by axial force ($P_{L)}$ and simultaneously, the bending die is moved by the force (Pu) perpendicular to the tube axis. The bending die is actively shifted by two servo motors in the X and Y directions, and the tipping around its center is done by a spherical connection of the bending die to the bearing. The pusher that feeds the tube in the Z direction is thereby synchronized with the X and Y axes of the bending die. The size of Pu depends on the magnitude of the offset *U*. The bending moment (*M*) acts to bend the tube, which is calculated by Eq. (1):

$$M = Pu \times A + PL \times U\ [6] \quad (1)$$

## 2.2 Process analysis of free-bending

For the typical free-bending forming process, the forming of any bending tube usually has three sections. In the section 1, the spherical bearing moves from the origin position to a predetermined offset position, the translation and rotation of the bending die is held as long as the offset increases correspondingly. Then, the bending die reaches the maximal position and an arc has been formed which is a part of the entire bending tube. In section 2, the bending die keeps in the maximal position to form complete the rest of the bending tube and meanwhile, the tube is kept feeding till the required bending angle is completed. During the section, the offset of the bending die is a constant value $U_{max}$ which is determined by the required R. In section 3, the bending die declines to its end position as the offset decreases; at the beginning, the tube has already the required bending radius (*R*) and bending angle (θ) and the fed tube is not bent in this section [15]. Sections 1 and 3 are considered as transition sections in the bending forming process while section 2 is called the arc section. As shown in Fig. 2, the length of the fed tube in the three sections of the bending tube and two straight lines were $S_1$, $S_2$, $S_3$, $L_1$, and $L_2$, respectively.

For a complex bending component in the three dimensions, its shape is decided by the length of straight lines (*L*), the bending radius (*R*), and bending angle (θ) of each bend and the relative position of bending planes. When forming straight sections, the value of the offset of the bending die is 0, and the axial feeding length of the tube is the length of straight lines (*L*). The bending radius (*R*) of the tube is decided by the

**Table 1** Bending program

| G | X (mm) | Y (mm) | Z (mm) | F (mm/s) | M |
|---|---|---|---|---|---|
| G01 | – | – | 36.000 | 10.000 | – |
| G01 | 3.131 | 5.423 | 30.864 | 10.000 | – |
| G01 | − 3.131 | −5.423 | 30.864 | 10.000 | – |
| G01 | – | – | 86.946 | 10.000 | M02 |

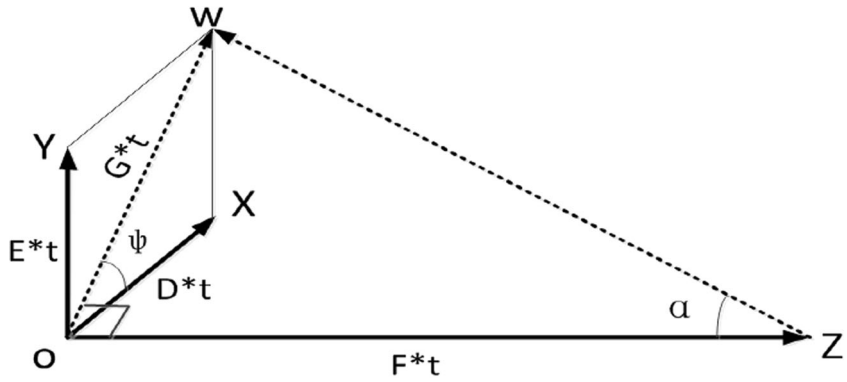


**Fig. 6** Calculation of the moving rate of the bending die

magnitude of offset $U_{max}$ and approach $A$, which is calculated by Eq. (2):

$$\mathrm{Umax} = R\left(1-\sqrt{1-\left(\frac{\mathrm{A}}{\mathrm{R}}\right)^2}\right) \tag{2}$$

The motion trace scope of the bending die is the circle of radius $U_{max}$ centered at initial position in the X-Y plane. The magnitude of the speed ($u$) of the bending die in sections 1 and 3 is not a constant value while the feed rate ($v$) of the tube in the Z-direction is fixed during the complete bending process [15]. By calculating the tipping angle ($\Phi z$) of the bending die, the speed of the bending die can be obtained using Eqs. (3) and (4):

$$\mathrm{u_1} = \frac{\mathrm{v}}{\mathrm{R}\left(\cos\frac{\mathrm{vt1}}{\mathrm{R}}\right)^2}\left[\mathrm{A}-\mathrm{Rsin}\frac{\mathrm{vt1}}{\mathrm{R}}\right] \quad \Phi z = \frac{\mathrm{vt1}\times 180}{\pi\times \mathrm{R}}$$
$$\text{for } 0 < \mathrm{vt_1} < \mathrm{S_1 with}\ \ \mathrm{S_1} = \frac{\pi\times \mathrm{R}\times \mathrm{arcsinA/R}}{180} \tag{3}$$

$$\mathrm{u_3} = \frac{(\mathrm{vt3}-\mathrm{A})\times \mathrm{V}}{\mathrm{R}\sqrt{1-\frac{(\mathrm{A}-\mathrm{vt3})^2}{\mathrm{R}^2}}} \quad \Phi z = \arccos\sqrt{1-\left(\frac{\mathrm{A}-\mathrm{vt3}}{\mathrm{R}}\right)^2}$$
$$\text{for } 0 < \mathrm{vt_3} < \mathrm{S_3 with}\ \mathrm{S_3} = \mathrm{A}[15] \tag{4}$$

However, according to the accomplished bending experiments, the kinematical and mathematical calculations between the offsets and the bending radii represent only the theoretical value of the curvature of the bending line which varies with the material of the tubes. Therefore, the bending radius $R$ varies even though the offset $U$ does not change. In order to achieve the required radius in simulation and experiments, the offset of the bending die needs to be provided with a material correction factor (Km). However, the Km is not a constant value and changes as a result of varying the materials properties of tube such as Young's modulus, strength characteristics, spring back behavior, hardening properties, and so on [17]. This problem is also described by Gantner who found a correction factor of 1.63 for stainless steel and 1.59 for aluminum

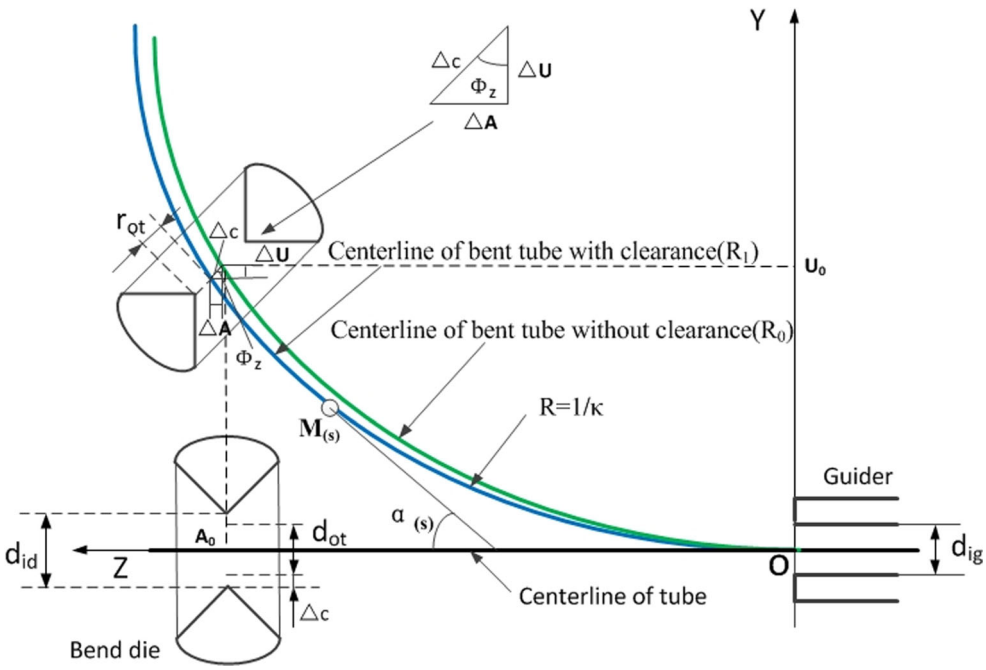


**Fig. 7** Comparison of the centerline of bent tube

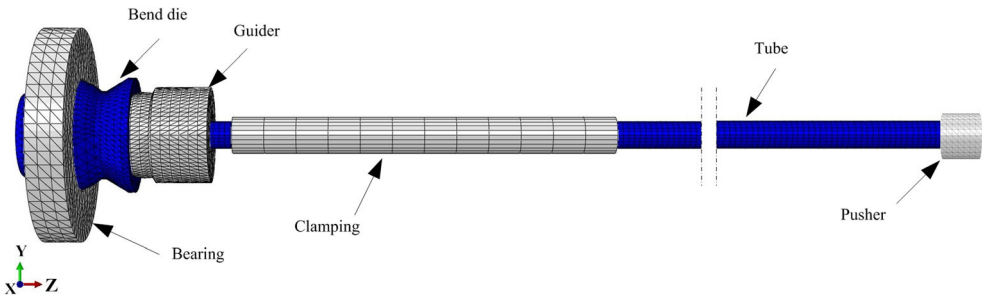


**Fig. 8** FE model of three-axis free-bending system

is necessary to match the bending radius of the bending tests by the FE simulation [18]. In this investigation, the correction factor for copper is calculated by comparing the simulation results with the mathematical model repeatedly. After the bending radius ($R$) has been determined, the bending angle (θ) of the tube depends on length $S_2$. It can be determined by Eq. (5):

$$S_1 + S_2 = S_1 + vt_2 = \frac{\pi \times \theta \times R}{180} \tag{5}$$

The bending direction defined as the angle (ψ) with the X axis of the bending die in the X-Y plane that determines the relative position of each curved plane directly. The bending direction of the n-th bending in the X-Y plane is related to the bending direction of (n-2)-th, (n-1)-th, (n + 1)-th bending, and the included angles of them on the X-Y plane. As represented in Fig. 3a, the straight part of tube Pn-1-Pn (Pn and Pn-1 are cross points of two straight parts) is overlapped upon the Z axis of the input coordinate axis by revolution around the point Pn-1. Thus, as shown in Fig. 3b, the angle between the straight part of tube Pn-Pn + 1 and the straight part of tube Pn-1-Pn is the included angle of the two curved plane of the bend Pn-1 and the bend Pn. Then, the bending direction of n-th bending on the X-Y plane can be calculated using Eq. (6) [19]. Based on the bending direction, as shown in Fig. 3c, the offset of the bending die of n-th bending in X and Y directions can be calculated using Eq. (7):

$$\psi_n = \psi_{n-1} + (\psi_{nn+1} - \psi_{n-1n-2}) \tag{6}$$

$$Ux_n = Umax_n \times \cos\psi_n, Uy_n = Umax_n \times \sin\psi_n \tag{7}$$

## 2.3 CNC control of free-bending forming

As depicted in Fig. 4, in the three-axis free-bending forming system, the control of the servo motors in the X and Y directions and the chain to forward the pusher is done by a CNC System. The bending program is based on the input bending data including approach ($A$), feeding velocity ($v$), straight length (Ln), bending radius (Rn), bending angle (θn), and bending direction (ψn). The chart for entering the bending data is shown in Fig. 5. After entering the data, appropriate offsets and feeding lengths are computer calculated and the bending program corresponding to a bent product can be obtained. As shown in Table 1, there is an easy program based on the data from Fig. 5 without any correction:

- G01 means normal operation
- X means X coordinates of the bending die in X-Y relative coordinate system
- Y means Y coordinates of the bending die in X-Y relative coordinate system
- Z means feeding length of the tube in the Z-direction
- F means feeding rate of the tube in the Z-direction
- M02 of end line is the ending of the bending operation

In this program, the X and Y coordinates of the bending die in the X-Y absolute coordinate system can be calculated by Eqs. (8) and (9):

$$X = Umax \times \cos\psi = R\left(1 - \sqrt{1 - \left(\frac{A}{R}\right)^2}\right) \times \cos\psi$$
$$= 75\left(1 - \sqrt{1 - \left(\frac{30}{75}\right)^2}\right) \times \cos 60^\circ = 3.131\text{mm} \tag{8}$$

$$Y = Umax \times \sin\psi = R\left(1 - \sqrt{1 - \left(\frac{A}{R}\right)^2}\right) \times \sin\psi$$
$$= 75\left(1 - \sqrt{1 - \left(\frac{30}{75}\right)^2}\right) \times \sin 60^\circ = 5.423\text{mm} \tag{9}$$

**Table 2** Material parameters setting

| Material | Density (kg/m$^3$) | Elastic modulus (Gpa) | Yield strength (Mpa) | Poisson's ratio |
|---|---|---|---|---|
| TP1 | 8900 | 110 | 294 | 0.32 |
| YG8 | 14,500 | 71 | 2451 | 0.30 |

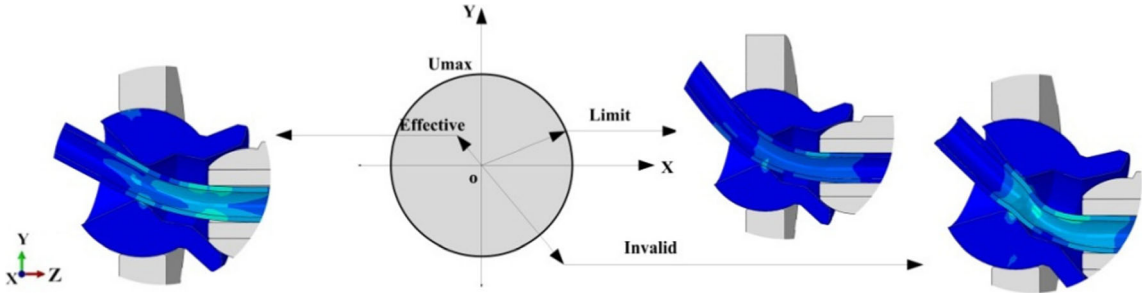


**Fig. 9** Motion trace scope of bending die

The feed rate ($F$) in the Z-direction is constant during the complete bending process and is synchronized with the X and Y axes of the bending die. Figure 6 illustrates the moving speeds ($D$ and $E$) of the die, which can be determined using Eqs. (10–14) as:

$$\tan\alpha = \frac{\mathrm{G}\times\mathrm{t}}{\mathrm{F}\times\mathrm{t}} = \frac{\mathrm{G}}{\mathrm{F}} = \frac{OW}{OZ} = \frac{\sqrt{OX^2+OY^2}}{OZ} \tag{10}$$

$$\mathrm{G} = \frac{F\times\sqrt{\mathrm{OX}^2+\mathrm{OY}^2}}{\mathrm{OZ}} = \frac{10\times\sqrt{3.131^2+5.423^2}}{30.864} = 2.028\mathrm{mm/s} \tag{11}$$

$$\mathrm{D} = \mathrm{G}\times\cos\psi = 2.028\times\cos60^\circ = 1.014\mathrm{mm/s} \tag{12}$$

$$\mathrm{E} = \mathrm{G}\times\sin\psi = 2.028\times\sin60^\circ = 1.756\mathrm{mm/s} \tag{13}$$

## 2.4 Key parameters of three-axis free-bending forming

The core of the free-bending forming technology is the movement curves of the bending die in the bending process which is influenced by several factors such as the stress-strain state, cross-section deformation of the tube, and friction between the tube and die resulting from the forming process and the die geometry. Key parameters of the 3D free-bending forming are as follows which are vital important for forming quality and accuracy.

The first parameter is the clearance, between tube and bending die (Δc). The 3D free-bending of the tube is a complex deformation process under the coupling of multi-factors. The clearance of different parts of the tube and dies seriously affects the uneven flow of the materials [20]. In the bending process, the tube is subjected to the multi-direction joint constraint of the bending die, the guider, and the pusher. The clearance between the tube and the die changes the stress-strain state of the local and global deformation domain. During the bending process, the outer profile of the tube after bending is subjected to axial tensile stress while the inner profile is subjected to axial compressive stress. Therefore, it is inevitable that the thickness of the outer wall thickness will be reduced and the thickness of the inner wall will be increased. Under a low value of the clearance, there may be a compression wrinkling in the tube forming area. However, if the clearance value is huge, the geometry precision of the components will influenced by the unstable contact between tubes and dies. As depicted in Fig. 7, the centerline of tube can

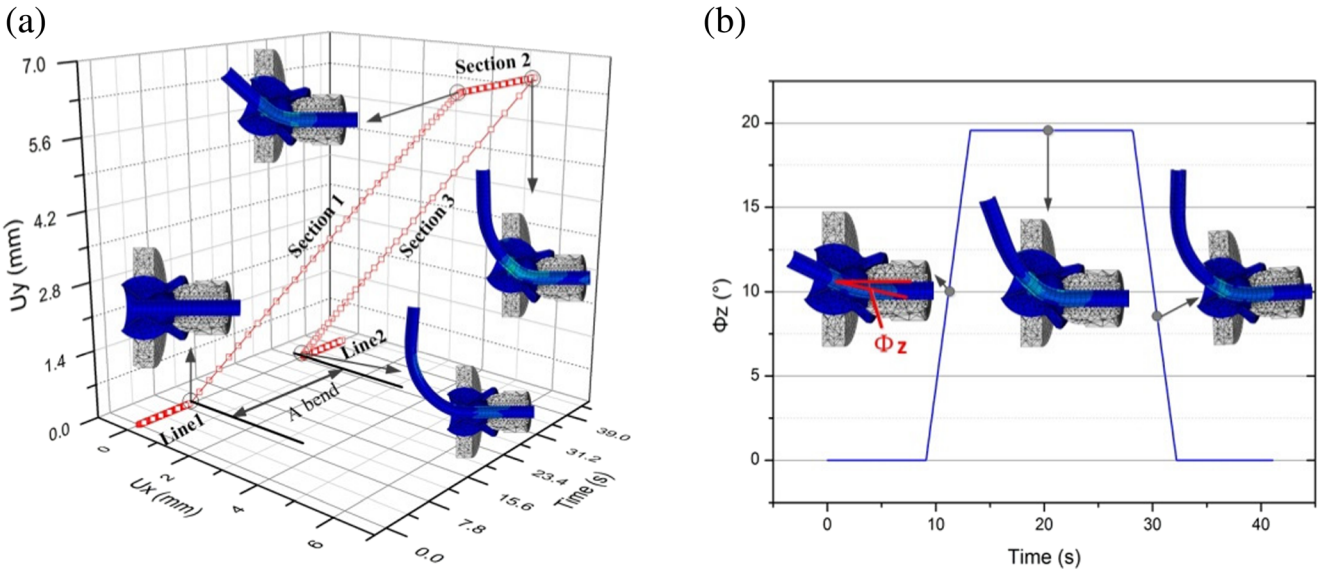


**Fig. 10** Movement curves of bending die for a bend: **a** the offsets in X and Y directions; **b** the tipping angle Φz around the center

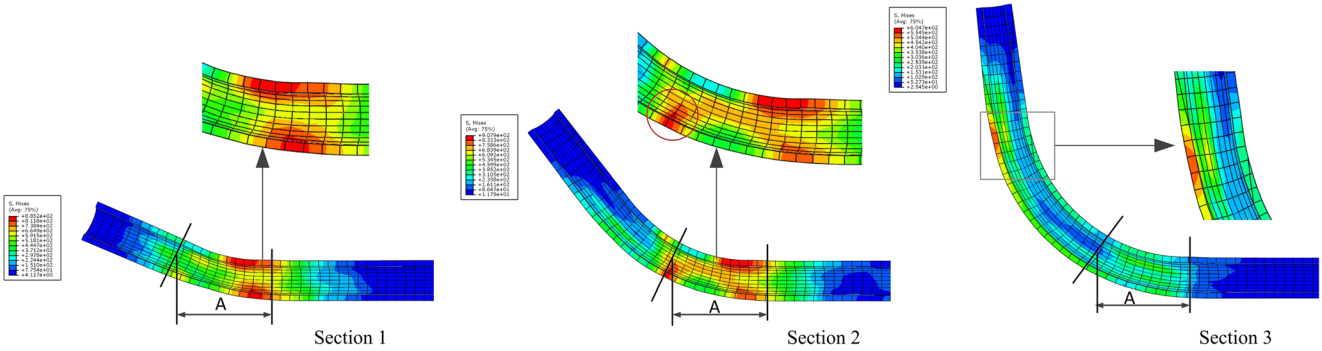


**Fig. 11** Stress variation in the free-bending process

be influenced by the clearance. It is assumed that the inner diameter of the guider ($d_{ig}$) is equal to the outside diameter of the tube ($d_{ot}$). The clearance will make the centerline of the tube downward; thus, the actual offset of the bending die and the approach A will change accordingly. Based on Eq. (2), the radius ($R_1$) of the centerline of the bent tube with clearance and the vector **M**(s) of the centerline of the tube can be calculated by Eqs. (14–17):

$$\Delta U = \Delta C \times \cos\Phi z \tag{14}$$

$$\Delta A = \Delta C \times \sin\Phi z \tag{15}$$

$$R_1 = \frac{(A_0 + \Delta A)^2 + (U_0 - \Delta U)^2}{2(U_0 - \Delta U)} \tag{16}$$

$$\mathbf{M}(s) = \begin{bmatrix} \Delta A \\ \Delta U \end{bmatrix} + \int_0^s \begin{bmatrix} cos\alpha_{(l)} \\ sin\alpha_{(l)} \end{bmatrix} dl \quad \text{for} \quad \alpha_{(s)} = \int_0^s \kappa(l) dl \tag{17}$$

where $\kappa$ = curvature (1/m), $s$ = arc length (mm), and $\alpha$= deflection angle (deg).

Due to the visible difference in the bending radius and the centerline of the tube under different clearances, another correction factor need be added whether in simulation or experiments. Therefore, in order to reduce the trend of wrinkling in the forming area and ensure the precision of the required components, reasonable clearance values between tubes and the bending die need to set before the free-bending forming process.

The second parameter is the distance between the center of the bending die and the exit of the guider (approach A). Based on Eq. 2, the $U$ value increases by increasing of $A$ value under the certain bending radius. The $A$ value has a vital effect on the forming quality and forming precision of tube fittings since the offset of the bending die and its movement curve are related to the approach A. If the $A$ value is too small, the reduced value of the offset leads to the decrease of the length of the deformation zone for the tube. During the bending process, the buckling of the inner profile of the bend tube and section distortion of the tube is very easy to occur. While the $A$ value is huge, the minimum bending radius of the tube would be increased and unable to fulfill the desired requirements. Accordingly, it is necessary to investigate the value of approach A as a parameter fixed before bending to guarantee the quality and precision.

The third parameter is the axial push velocity ($v$) of the tube. For the free-bending forming machine, the compression mechanism exerts radial pressure on the tube and the tube is formed under the combined action of the bending die and the pusher. The movement speed of the bending die has a certain matching relationship with $v$. In the simulation and experiments, $v$ is assumed as a constant value for simplicity. According to Eqs. (3) and (4), the decrease of $v$ value results in the slow movement of the bending die, and the forming efficiency is lower. On the

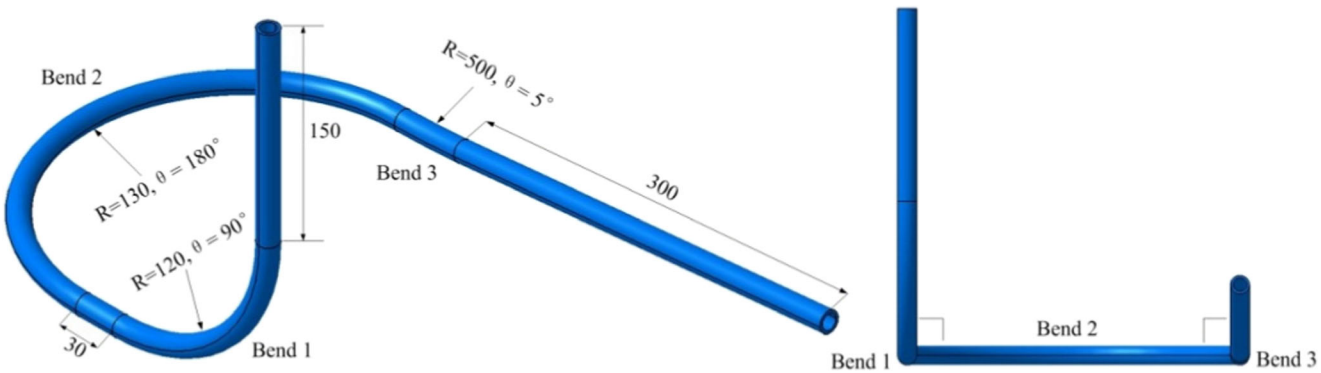


**Fig. 12** Copper tubular component and its geometrical dimension

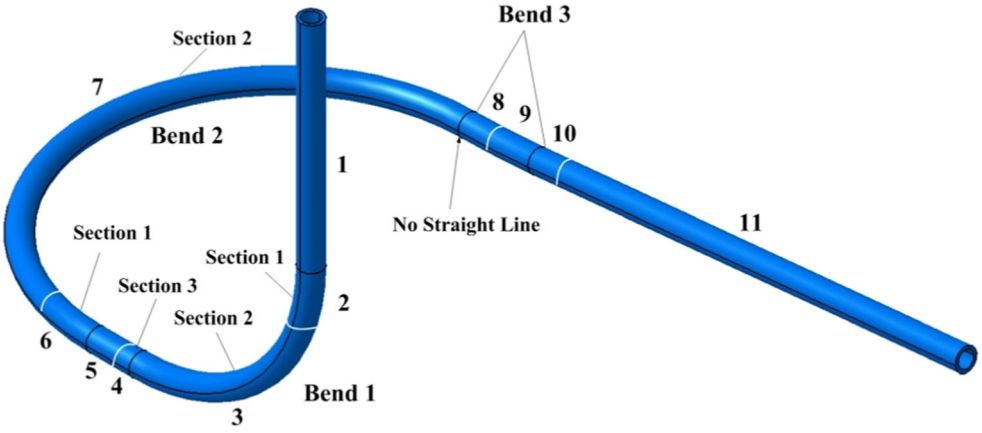


**Fig. 13** Sections of the forming process for copper tubular component

other hand, if the $v$ value is huge, it is easy to cause axial instability of the tube during the bending process.

## 3 Finite element analysis of the free-bending process

### 3.1 Finite element model

In order to investigate the free-bending process of profile and tube, ABAQUS/explicit finite element code was used to conduct numerical simulation of the forming process. The CAD model of this study including the tube, bending die, bearing, guider, clamping, and pusher of was accomplished by the CATIA software, then imported to the ABAQUS/explicit FE code, as depicted in Fig. 8. The materials of the tube and other parts were copper TP1 and alloy YG8, respectively. The relevant parameters are shown in Table 2. The tubular blank was dispersed into C3D8R solid elements which were eight-node linear brick, and reduced integration elements and other parts were defined as rigid bodies with R3D4 elements type. The analysis step was adjusted to dynamic explicit and the interaction was set to general contact. Since the bending die and the guider are ceramic tools, and the lubrication unit was designed near the bending die. Thus, the coefficient of friction between tools and the tube was very low [21]. Gantner investigated the influence of friction on the geometrical bending results of free-bending. The accomplished simulation results had found that the friction coefficients of $\mu = 0.02$ up to $\mu = 0.1$ has shown only insignificant effects with differences in the range of 2% for the bending radius, approx. 1% for the bending angle, and 0.4% in the wall thickness [22]. In this model, the coefficient of friction between the tools and the copper tubes was assumed to be 0.02. The guider and clamping are

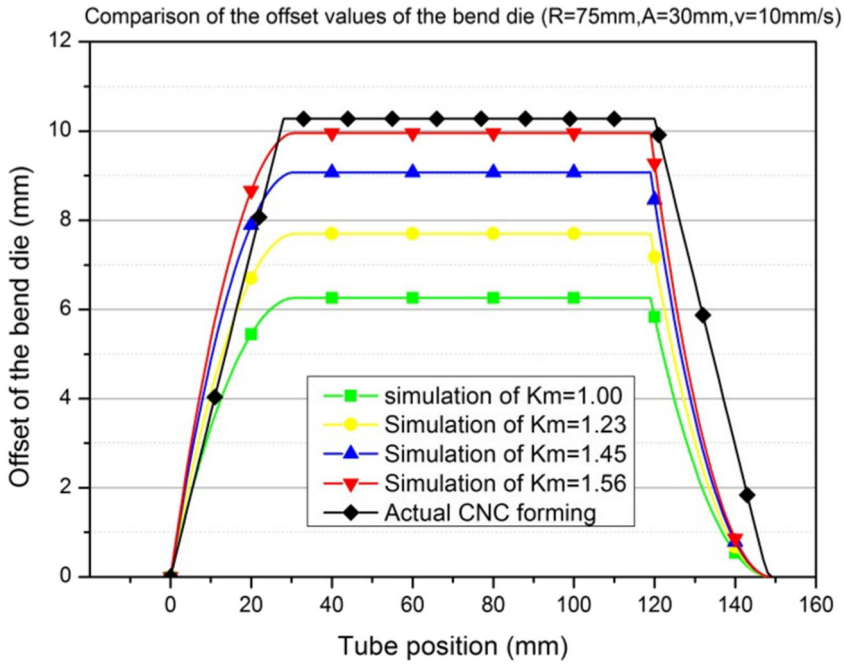


**Fig. 14** Comparison of the offset values of the bending die

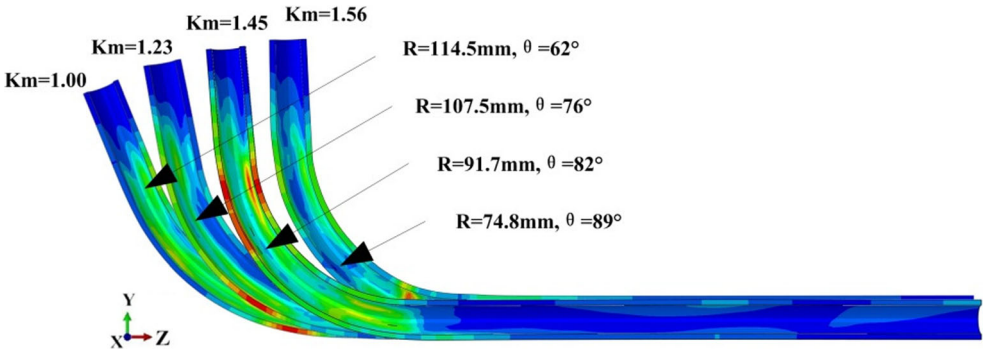


**Fig. 15** Simulation results of copper tube under different correction factors

**Table 3** Comparisons of numerical simulation results under different Δc value

| Clearance | Δc = 0.00 mm | Δc = 0.10 mm | Δc = 0.25 mm | Δc = 0.40 mm |
|---|---|---|---|---|
| Offset (mm) | 9.76 | 9.76 | 9.76 | 9.76 |
| Bending radius (mm) | 74.8 | 83 | 92 | 101 |
| Equivalent stress | | | | |
| Equivalent strain | | | | |
| Maximum wall thickness varying ratio (%) $(t' - t0)/to \times 100\%$ | + 9.1/− 6.1 | + 8.0/− 4.9 | + 4.5/− 4.0 | + 3.7/− 4.2 |
| Maximum ovalization (%) $(Dt - Dr)/Do \times 100\%$ | 7.33 | 7.43 | 7.59 | 7.75 |

set to encased. The pusher was set a specified movement speed in the Z direction, and the remaining degrees of freedom were all fixed. The bearing was set two movements respectively in the X and Y direction, and the remaining degrees of freedom were all fixed while the tube was not set load.

## 3.2 Motion trace scope and movement curves of the bending die

As mentioned previously, the motion trace scope of the bending die is the circle of radius $U_{max}$ centered at the origin on the X-Y plane. The bending die moves to any position in the circle from the origin where the tube can be bent to an arbitrary arc with a radius greater than the minimum bending radius, and the inner circular region is called the forming effective area. The minimum bending radius of the tube is formed when the bending die is on the circle and the circle line is defined as the forming limit zone. While the bending die moves to the outside of the circle, serious wrinkling and cross-section distortion will appear in the forming zone of the tube due to the ultimate bending strength and this part is named the forming invalid zone. In order to illustrate the point, simulations under different offsets of the bending die were carried out as depicted in Fig. 9. Simultaneously, the simulation of a right

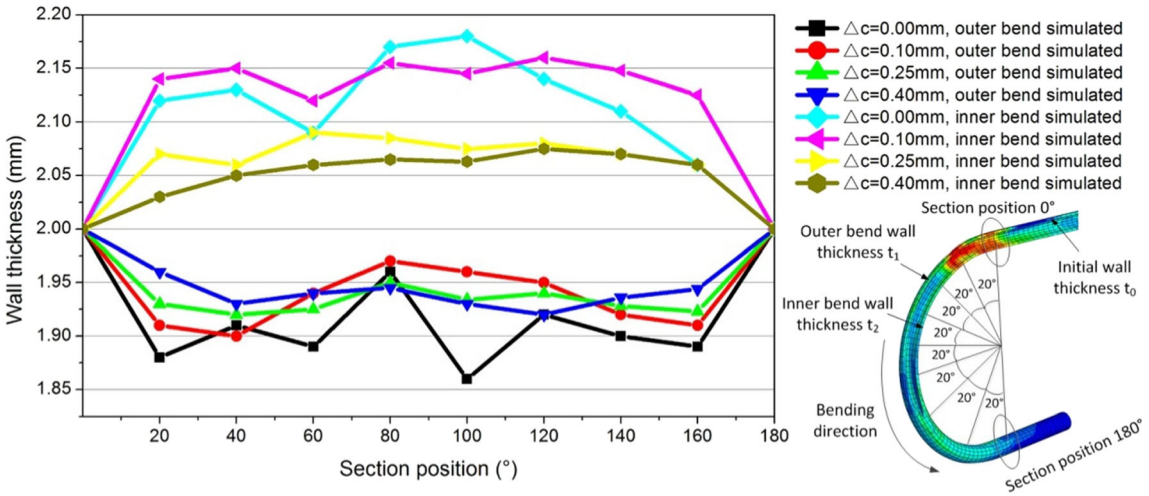


**Fig. 16** Comparison of the wall thickness from simulation at different Δc values

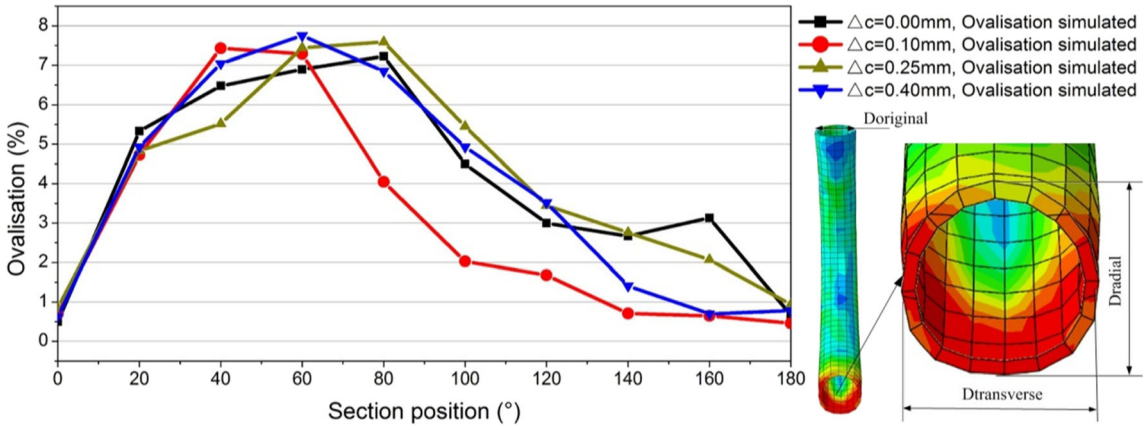


**Fig. 17** Comparison of the ovalization from simulation under various Δc value

angle bend was implemented to reveal movement curves of the bending die including the curves of the offsets and the tipping angle (Fig. 10).

### 3.3 Stress variation in the free-bending process

In the free-bending process, the bending deformation zone of the tube is between the center of the bending die and the front of the guider. The horizontal length of the bending deformation zone is equal to the *A* value. Figure 11 shows the stress variation in three sections of the free-bending process. In section 1, under the driving of the bending die, the tube is formed from the front of the guider, and the inner and outer profiles of bend tubes at this area have a large stress. In section 2, the bending die remains stationary and the vertical compressive stress is applied to the outer profile of the bend tube. Therefore, the outer profile of the bend tube in the bending die also exhibits high stress. In section 3, the bending arc has been formed and the bending die and the guider do not exert any force on the tube. However, the outside of the tube is still subjected to tangential tensile stress; the stress concentration occurs at the outer profile of bend tube. From what has been analyzed above, it is the outer profile of the bend tube that the bending die exerts force on and theoretically the force acts only at a one point on the outer profile of the bend tube.

## 4 Free-bending process design of copper tubular components

### 4.1 Geometric analysis

In this study, the free-bending process of the copper bending tubular component used in the refrigerator of the atomic pore generator was investigated using the numerical method through the ABAQUS finite element code to prove the

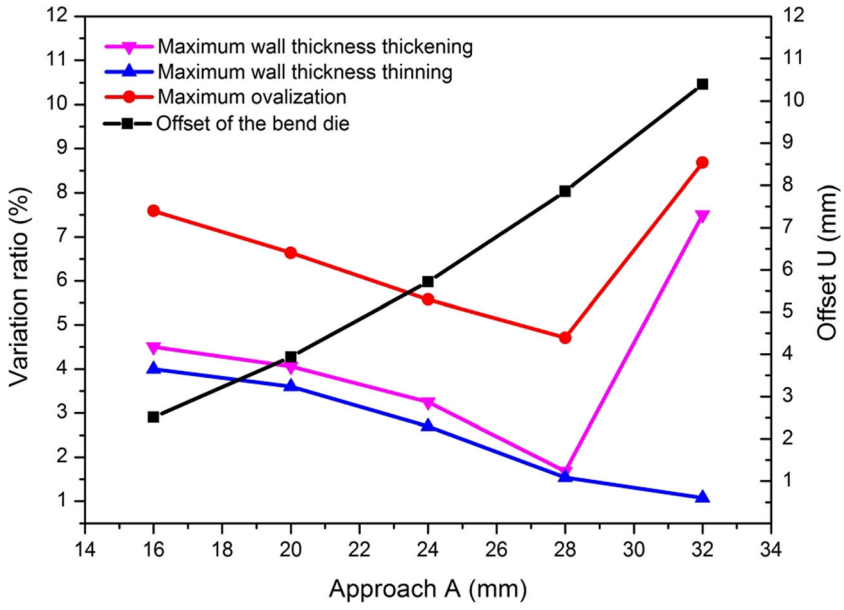


**Fig. 18** Comparisons of from simulation at different *A* values

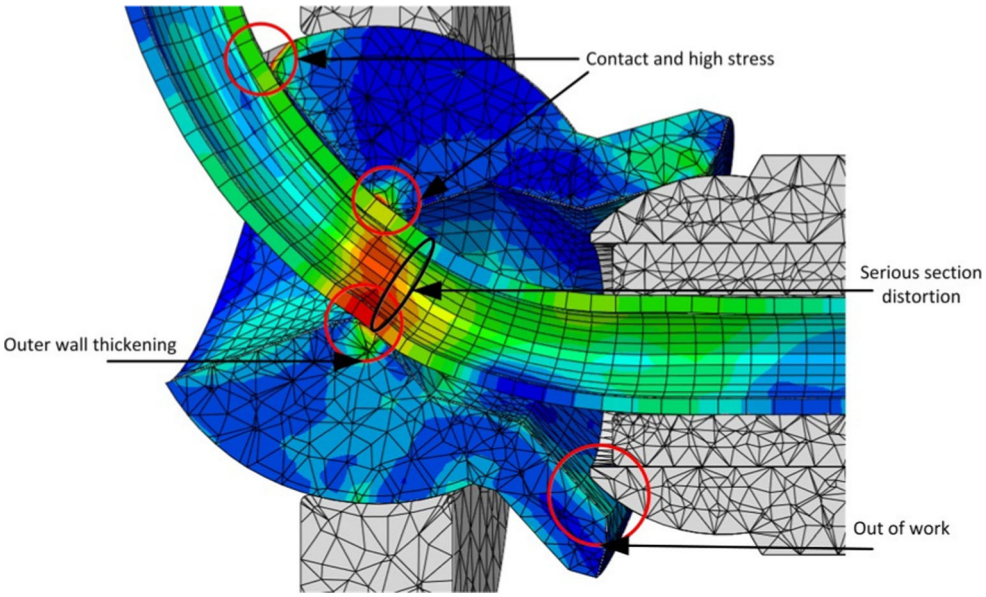


**Fig. 19** Forming defects at *A* value of 32 mm

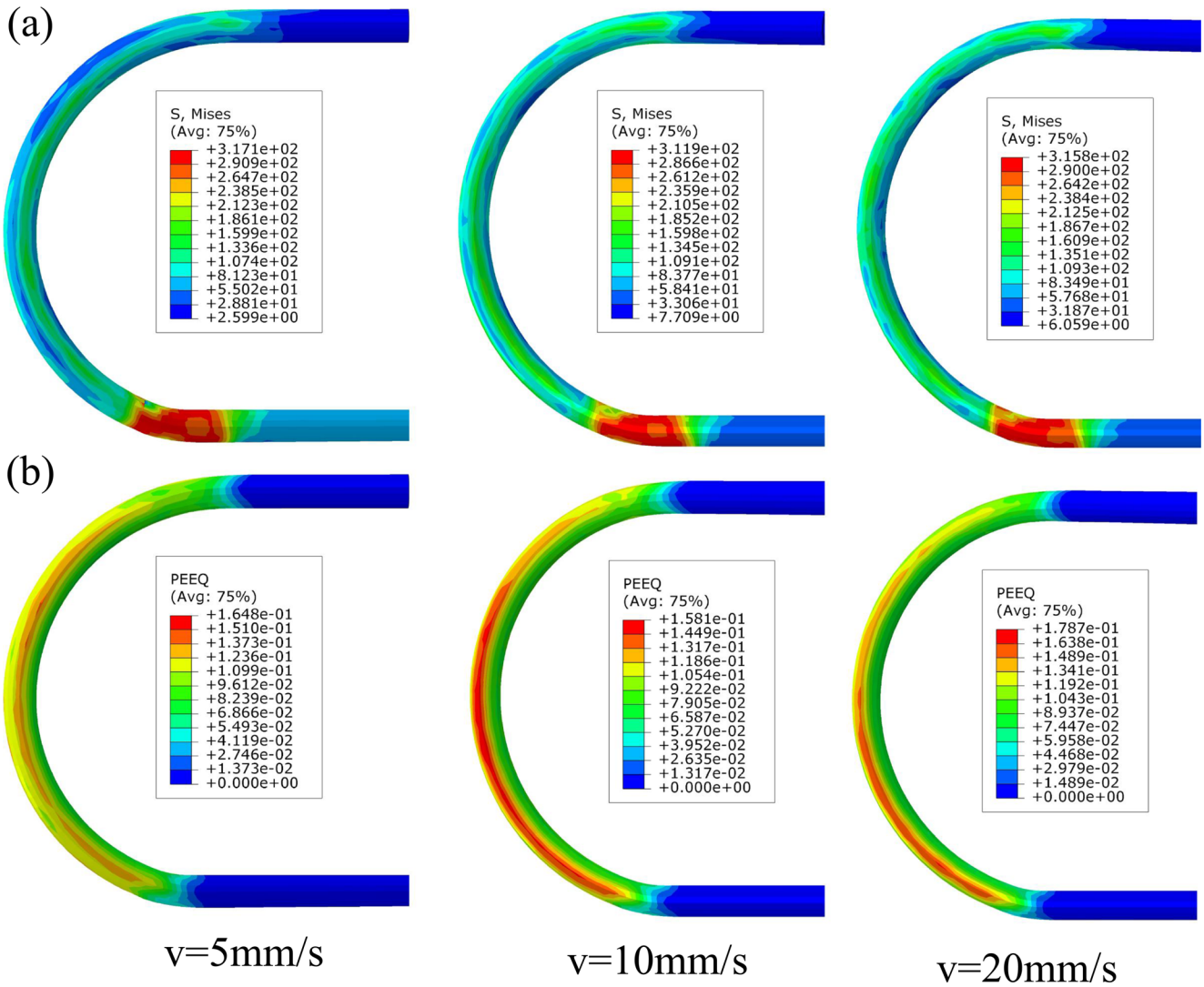


**Fig. 20** Equivalent stress and strain of bending results at different *v* values

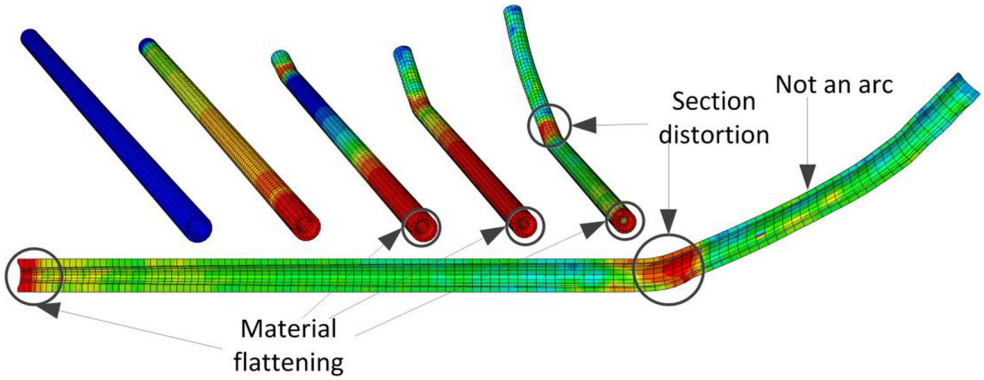


**Fig. 21** Bending result at *v* value of 400 mm/s

accuracy of the process analysis above. Figure 12 shows the CAD model of the tubular component. The diameter of the tubular component is 16 mm, the wall thickness is 2 mm, and the axial length is 1120 mm. In order to obtain reasonable forming process parameters, the influence of clearance (Δc), approach A, and speed v on the forming quality was studied under the condition of the same bending radius.

This bending component represents a complex spatial bending shape with three bending planes. The bending plane 1 is parallel to the bending plane 3 and is perpendicular to the bending plane 2. The bending radius and bending angle are different in the three bending planes. Without changing the bending die, the tubes cannot be shaped into this structure within a cycle by traditional bending technologies due to the continuous varying bending radii and angles in different bending planes. And if multi-steps forming is carried out, there may be serious cross-section distortion and accumulative geometry dimension errors. However, the free-bending forming technology can accurately form the component without changing the die and reclamping tube. As described previously in section 2.1, the bending tube is usually divided into three sections. Therefore, in order to formulate the complete parameters of the forming process, it needs to be segmented into 12 sections including nine (3 × 3) sections of three bends and three sections from three straight lines. However, since there is no straight line between bend 2 and bend 3, the section 3 of bend 2 is nonexistent and the final number of the total sections is 11, as shown in Fig. 13.

## 4.2 Material correction factor (Km) of copper

In conventional bending processes such as push bending and rotary draw bending, the final forming geometry is defined by the geometry of the bending die; thus, there is no obvious difference on the dimension between different materials. On the other hand, in the free-bending process, the final forming geometry is decided by the offset of the bending die and the tube is not subject to multiple constraints unlike traditional bending processes. Therefore, the different material parameters such as strength characteristics, springback behavior, and hardening properties will lead to different springback behaviors and deformation of cross-section which deviate the results from the results obtained by kinematical and mathematical calculations. In order to achieve the required bending radius and angle in simulations and experiments, the offset of the bending die ($U$) should be provided with a correction factor, Km, belong to copper. The new offset of the bending die ($U_{(m)}$) affected by tube materials can be calculated with Eq. (18). In order to obtain the value of Km, the basic simulation of $Km_0 = 1$ for the required radius $R_0$ was carried out without considering the effect of clearance ($\Delta c = 0$) and the radius R' from the simulation result was measured. Therefore, the correction factor Km can be calculated as follows:

$$U_{(m)} = \text{Uanalysis} \times \text{Km} \tag{18}$$

$$\text{Uanalysis(Ro)} = \text{Uanalysis}\left(R'\right) \times \text{Km} \tag{19}$$

$$U_{(m)}(R_0) = \text{Uanalysis(Ro)} \times \text{Km} \tag{20}$$

$$\text{Km} = U_{(m)}(R_0)/\text{Uanalysis(Ro)} = \text{Uanalysis(Ro)}/\text{Uanalysis}\left(R'\right) \tag{21}$$

$$\text{Km(copper)} = \frac{75\left(1-\sqrt{1-\left(\frac{30}{75}\right)^2}\right)}{114.5\left(1-\sqrt{1-\left(\frac{30}{114.5}\right)^2}\right)} = 1.56 \tag{22}$$

$$U_{(m)}(R = 75\text{mm}) = 75\left(1-\sqrt{1-\left(\frac{30}{75}\right)^2}\right) \times 1.56 = 6.26 \times 1.56 = 9.76\ \text{mm} \tag{23}$$

**Table 4** Optimum parameters used in the simulation of the tubular component

| Parameter | Km | Δc (mm) | Kc | A (mm) | v (mm/s) |
|---|---|---|---|---|---|
| Value | 1.56 | 0.25 | 1.24 | 28 | 10 |

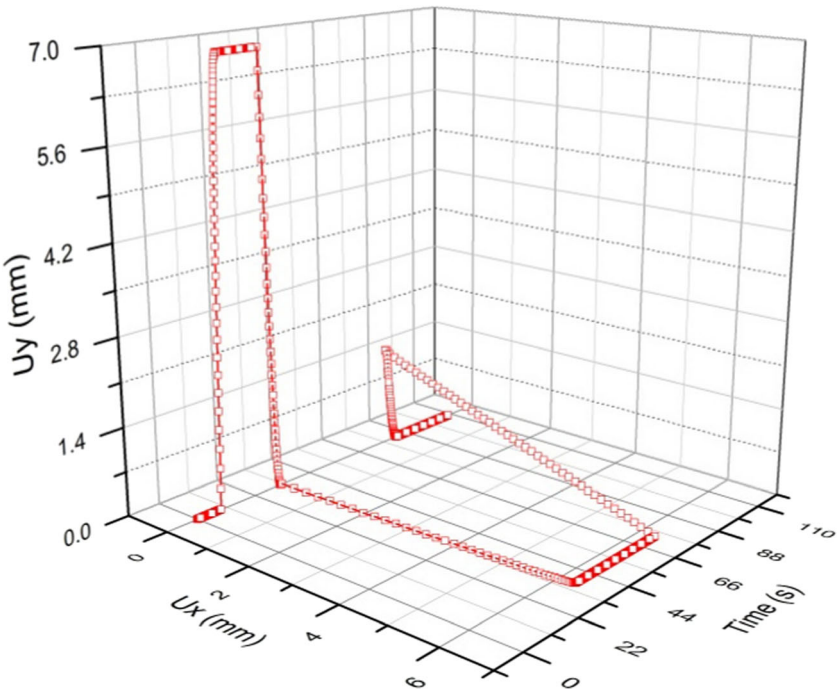


**Fig. 22** Offset curve of the bending die for the copper tubular component

Figure 14 depicts the comparison of the offset values of the bending die under different Km values of copper in simulation and from the CNC controller of the bending machine. The required radius of the tube with 2 mm in thickness is 75 mm, and required bending angle θ is 90°. From both simulation and calculation results and which were obtained using Eqs. (19)–(21), the final tube matches the required geometry most with a correction factor of 1.56, as shown in Fig. 15. The resultant difference for the maximum deflection between the machine controller and the simulation of Km = 1.56 input of 0.45 mm can be attributed to the stiffness of the machine setup and some clearance between the tube and the tools since in simulation the tools are modeled as rigid bodies without any deformation [13].

### 4.3 Optimal value of clearance and corresponding correction factor (Kc)

The clearance between the tube and the bending die has a huge influence on the final forming results for the three-axis free-bending forming. Table 3 shows numerical simulation bending results and its forming quality index under different Δc value. Since the *A* value was fixed, the offset values of the bending die under different Δc value are equal which could be calculated using Eqs. (2) and (13). However, from the theoretical analysis above and simulation results, it could be concluded that the bending radius increased as the clearance increased. When the Δc value was equal to 0.40 mm, the bending radius reached 101 mm. This phenomenon could be attributed to the decrease of the actual offset of the bending die

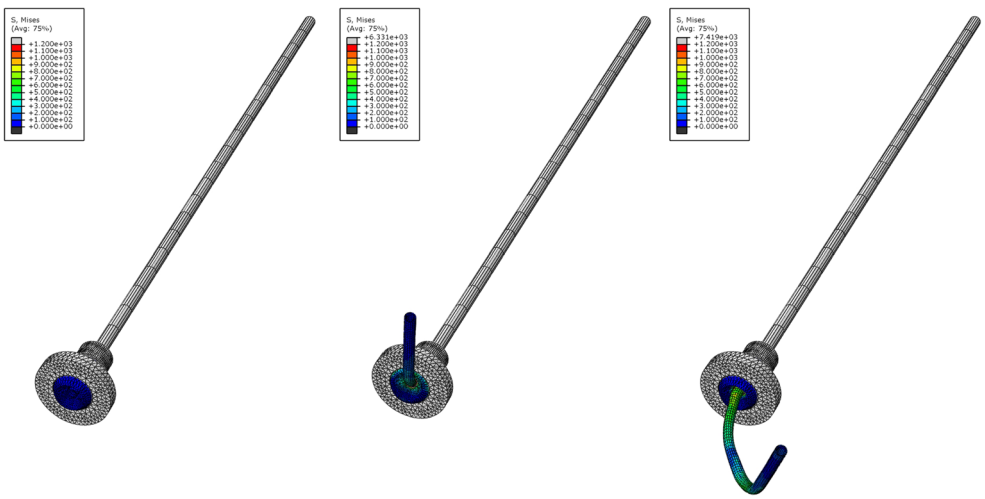

**Fig. 23** FE Simulation of forming process under optimal parameters

**Table 5** Comparison for the shape of the tube

| CAD model |
|---|
| Simulation results |
| Test results |

because it had to move a distance to contact the tube at the beginning of the bending process. Thus, in order to achieve the required radius in simulation and experiment, the offset of the bending die need be provided with another correction factor (Kc) caused by the clearance:

$$\mathrm{U}(\mathrm{m},\Delta\mathrm{c}) = \mathrm{Uanalysis} \times \mathrm{Km} \times \mathrm{Kc} \tag{24}$$

$$\mathrm{Kc}(\Delta\mathrm{c}=0.25\mathrm{mm}) = \frac{\mathrm{Uanalysis(Ro)}}{\mathrm{Uanalysis}\left(\mathrm{R}'\right)} == \frac{6.26}{92\left(1-\sqrt{1-\left(\frac{30}{92}\right)^2}\right)} = 1.24 \tag{25}$$

To analyze the thickness distribution and the ovalization of the cross section in the tube, predefined positions (every 20° along the bend whereby the starting point was located where the tube was fed) in the bent tube from simulation results were selected. The comparison of the wall thickness and the ovalization from simulation under different Δc value were depicted in Fig. 16 and Fig. 17, respectively. It showed the result with a maximum ovalization of no more than 8%, a maximum wall thickness thinning ratio of about 6%, and a maximum wall thickness thickening ratio of about 9%. And the wall thickness varying ratio decreased with the increase of the clearance; therefore, the high uniformity of the wall thickness can be obtained at high clearance. However, the large clearance means instability during the work and large offset of the bending die which may exceed the working stroke. Thereby, the Δc value of 0.25 mm was selected for the final bending simulation of the component. Simultaneously, the calculation of the correction factor (Kc) for Δc = 0.25 mm was done according to the same principle of the calculation of Km and Eq. (16), and the obtained value was 1.24 using Eq. (25).

### 4.4 Optimal approach (*A*)

The *A* value is an important variable of the control of the bending die. Under the same bending radius and tube feed speed, the size of A affects the movement curve of the bending die and the forming quality of the tube. As depicted in Fig. 18, the maximum wall thickening and thinning ratio and the maximum ovalization decreased with the increase of the A value of 16–28 mm. This is due to the increase in both the horizontal and vertical length of the bending deformation zone. While the size of *A* value was 32 mm, the maximum wall thickening ratio and the maximum ovalization got very high. It could be attributed to the forming limit zone of the bending die, since a larger *A* value caused a larger offset of the bending die according to Eq. (2). The forming defects under *A* value of 32 mm is described in Fig. 19. From the stress cloud chart, the deformation of the bending die was visible. The inside and outside of the tube were load-bearing in contact with the bending die simultaneously and the thickness of the outer wall increased due to the extrusion which also created serious section distortion. Thereby, the *A* value of 28 mm was selected for the final bending simulation of the component.

### 4.5 Optimal feeding velocity (*v*)

It is not difficult to understand that the smaller the feeding speed is, the better the quality of the forming tube when the precision of the machine is high enough. But in the tube production, the speed must be raised to a certain value to ensure efficiency. In the bending test, the maximum feed speed can only be achieved to 20 mm/s, due to the limitation of our designed equipment. While the speed of 350 mm/s is the maximum speed of the most advanced free-bending equipment in the world. The equivalent stress and strain cloud chart of bending results under different *v* value (*v* = 5-20 mm/s) as shown in Fig. 20. Whether the stress and strain or the bending radius was conducted, there is little difference between those results. Because if the feed speed is too high (*v* = 400 mm/s), the tube was unable to form an arc and the Euler buckling

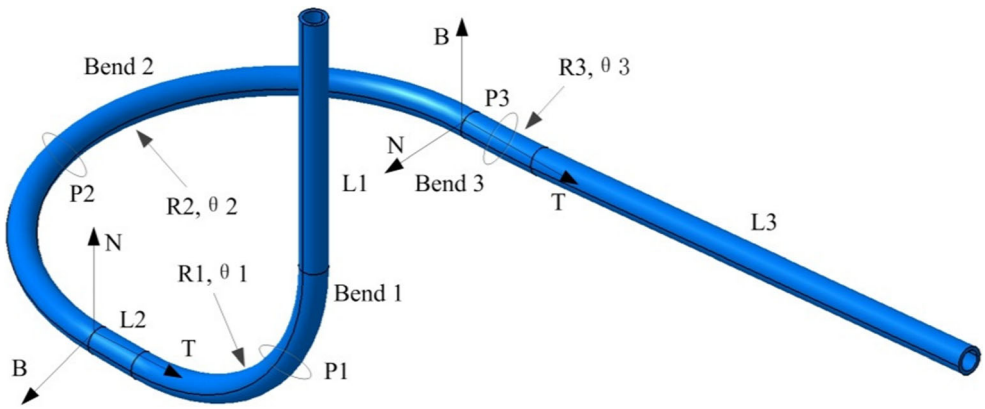


**Fig. 24** Schematic diagram of tube size and typical section of bending forming zone

**Table 6** Comparison for the dimension of the component

| | Bend 1 | | | Bend 2 | | | Bend 3 | | |
|---|---|---|---|---|---|---|---|---|---|
| | L1 (mm) | R1 (mm) | θ1 (°) | L2 (mm) | R2 (mm) | θ2 (°) | L3 (mm) | R3 (mm) | θ3 (°) |
| CAD | 150 | 120 | 90 | 30 | 130 | 180 | 300 | 500 | 5 |
| Simulation | 147 | 116 | 88 | 36 | 121 | 187 | – | 486 | 7 |
| Bending test | 156 | 128 | 93 | 39 | 137 | 191 | – | 520 | 10 |

**Table 7** Comparison for the torsion of the component

| | Desired | Simulated | Error (%) | Measured | Error (%) |
|---|---|---|---|---|---|
| Bend1-Bend2 | 477 | 320 | − 33.0 | 380 | − 20.3 |
| Bend2-Bend3 | 12 | 20 | +67 | 25 | + 108 |

phenomenon would occur at the end of the tube which caused material flattening. In addition, serious distortions at cross section appeared in the tube bending zone, as shown in Fig. 21. Thereby the $v$ value of 10 mm/s was selected for the final bending simulation of the component considering efficiency and quality.

### 4.6 Simulation of the copper tubular component

Based on the finite element simulation and analysis, the optimum parameters used in the simulation of the tubular component are summarized in Table 4. The correction factors (Km and Kc) are calculated by the data of the simulation results and the control parameters ($\Delta$c, $A$, $v$) are obtained from the comparison of the simulation results. Based on those parameters, the offset curve of the bending die and the simulation of the forming process were presented in Fig. 22 and Fig. 23, respectively.

## 5 Bending tests and comparison

Based on the mentioned simulation results, the actual bending test was accomplished on the self-developed 3D free-bending forming system. Table 5 presented the comparison for the shape of the formed tube, the CAD model, and the simulation results. The results showed that there is no significant difference on the shape of the tube.

The dimension and typical sections of the bending forming zone were represented in Fig. 24. The dimension of the formed component after the bending test was calculated by a special tool based on laser scanning technique and afterwards was compared with the data of the CAD model and the simulation results, as shown in Table 6. The results indicated that the size of the simulation and test are close to the design size, but the bending radius from the test was relatively larger than the simulation. It could be attributed to the clearance in the guider and bending die which was larger than that used in the design. However, low accuracy in the torsion of the component had been presented based on the proposed parameters and improvement of torsion is a target of future work. The torsion can be calculated by Eqs. (26–28) [23] and the data was shown in Table 7.

$$d\mathbf{T}/ds = \kappa\mathbf{N} \tag{26}$$

$$d\mathbf{N}/ds = -\kappa\mathbf{T} + \tau\mathbf{B} \tag{27}$$

$$d\mathbf{B}/ds = -\tau\mathbf{N} \tag{28}$$

where $T$ = the unit tangent vector, $N$ = the principal normal vector, $B$ = the assistant normal vector, $\kappa$ = curvature (1/m), $s$ = arc length (mm), and $\tau$ = torsion (deg/m).

**Table 8** Comparison for forming quality of the component

| | Simulation | | | Test | | |
|---|---|---|---|---|---|---|
| Typical sections | P1 | P2 | P3 | P1 | P2 | P3 |
| Ovalization (%) | 3.87 | 4.83 | 4.47 | 5.45 | 6.22 | 6.98 |
| Wall thickness varying ratio (%) | 2.05/− 1.85 | 3.23/− 4.76 | 1.75/− 2.24 | 4.21/− 6.58 | 6.22/− 8.87 | 3.53/− 7.16 |

Table 8 summarized the comparison of the simulation and the bending test results with respect to the forming quality of the component. The ovalization in three typical sections of the component was no more than 7%; furthermore, there was not a big difference between the simulation and bending test results. However, the wall thickness varying ratios obtained from the bending test were nearly twice that obtained from simulation. For the precise bending equipment, a mandrel for the tube was generally applied in the free-bending process to reduce the varying ratio of wall thickness.

## 6 Conclusions

(1) The process of complex tubular bent components with continuous varying radii and several bends of different radii were analyzed using the revised mathematical model. The motion trace and limit were graphically described, which provided the important guide to design the free-bending forming process.

(2) The precision and quality of the bent tube were controlled by optimization of the key free-bending forming process parameters (the material correction factor (Km), the clearance between the tube axis and bending die axis ($\Delta c$) and the correction factor (Kc) for the clearance, the distance between the center of the bending die and the head of guide sleeve ($A$), and the axial push velocity ($v$)). The forming process design of the copper tubular component demands the determination of the above parameters and the motion trajectory of the bending die.

(3) Simulation and bending test for the copper tubular component were accomplished based on the forming process design ($Km = 1.56$, $\Delta c = 0.25$ mm, $Kc = 1.24$, $A = 28$ mm, $v = 10$ mm/s). The experimental and finite element simulation results are in agreement with the CAD model. The bent component with high quality proved the accuracy of the process analysis and the numerical simulation.

**Acknowledgements** This study was supported by the China Aviation Science Foundation (No. 2016ZE52047).

## References

1. Gensch F, Gall S, Fahrenson C, Müller S, Reimers W (2016) Characterization of weld seam properties of extruded magnesium hollow profiles. J Mater Sci 51(8):3888–3896
2. Hermes M, Staupendahl D, Becker C, Tekkaya AE, Staupendahl D (2011) Innovative machine concepts for 3D bending of profiles and tubes. Key Eng Mater 473:37–42
3. Zhang C, Li H, Li M (2016) Detailed analysis of surface asperity deformation mechanism in diffusion bonding of steel hollow structural components. Appl Surf Sci 371:407–414
4. Heng L, Shi KP, Yang H, Tian YL (2012) Springback law of thin-walled 6061-t4 al-alloy tube upon bending. Trans Nonferrous Metals Soc China 22(Suppl 2):s357–s363
5. Guo XZ, Jin K, Wang H, Pei W, Ma F, Tao J, Kim N (2016) Numerical simulations and experiments on fabricating bend pipes by push bending with local induction-heating process. Int J Adv Manuf Technol 84(9):2689–2695
6. Murata M, Kuboki T (2015) CNC tube forming method for manufacturing flexibly and 3-dimensionally bent tubes. Springer, Berlin, pp 363–368
7. Liang JC, Song G, Fei T, Yu PZ, Song XJ (2014) Flexible 3D stretch-bending technology for aluminum profile. Int J Adv Manuf Technol 71:1939–1947
8. Gantner P, Harrison DK, Silva AKMD, Bauer H (2004) New bending technologies for the automobile manufacturing industry. Proc Int Matador Conf:211–216
9. Li P, Wang L, Li M (2016) Flexible-bending of profiles and tubes of continuous varying radius. Int J Adv Manuf Technol:1–7
10. Li P, Wang L, Li M (2016) Flexible-bending of profiles with asymmetric cross-section and elimination of side bending defect. Int J Adv Manuf Technol 87:1–7
11. Murata M, Ohashi N, Suzuki H (1989) New flexible penetration bending of a tube: 1st report, a study of MOS bending method. Trans Jpn Soc Mech Eng C 55:2488–2492
12. Murata M (1996) Effects of inclination of die and material of circular tube in MOS bending method. Trans Jpn Soc Mech Eng C 62: 3669–3675
13. Murata M (1996) Effect of die profile and aluminum circular tube thickness with MOS bending. J Jpn Inst Light Met 46:626–631
14. Gantner P, (2008) The characterisation of the free-bending technique. Glasgow Caledonian University
15. Gantner P, Harrison DK, De Silva AK, Bauer H (2007) The development of a simulation model and the determination of the die control data for the free-bending technique. Proc Inst Mech Eng B J Eng Manuf 221:163–171
16. Germany J. NEU freebending machine [EB/OL]. http://www.etaitech.com/about/? 118.html
17. Yang X, Choi C, Sever NK, Altan T (2016) Prediction of springback in air-bending of advanced high strength steel (dp780) considering young's modulus variation and with a piecewise hardening function. Int J Mech Sci 105(1–2):266–272
18. Gantner P, Bauer H, Harrison DK, Silva AKMD (2005) Free-bending—a new bending technique in the hydroforming process chain. J Mater Process Technol 167:302–308
19. Nissin Technical. See http://www.nissin-precision.com/english/sindex.html
20. Heng L, Yang H (2011) A study on multi-defect constrained bendability of thin-walled tube CNC bending under different clearance. Chin J Aeronaut 24(1):102–112
21. Neu J, Eins links, eins rechts (2004) One left, one right – free-bending with a CNC-5-axis-tube bending machine. Maschinen Markt das Industrie Magazin 49:22–23
22. Gantner P, Bauer H (2004) Fea—simulation of bending processes with ls-dyna
23. Arreaga G, Capovilla R, Guven J (2001) Frenet-serret dynamics. Classical Quantum Gravity 18(23):5065–5083